Electrochimica Acta 215 (2016) 550–555

Contents lists available at ScienceDirect

Electrochimica Acta

journal homepage: www.elsevier.com/locate/electacta

Unlocking the electrochemistry abilities of nanoscaled $Na_{2/3}Ni_{1/4}Mn_{3/4}O_2$ thin films

Qian Peng[a], Yang Liu[a], Yongzhou Luo[a], Zhongpin Zhou[a], Yan Wang[b,*], Hua Long[a], Peixiang Lu[a], Jinfang Chen[b], Guang Yang[a,*]

[a] School of Physics and Wuhan National Laboratory for Optoelectronics, Huazhong University of Science and Technology, Wuhan 430074, China
[b] School of Chemical Engineering & Pharmacy, Wuhan Institute of Technology, Wuhan 430074, China

ARTICLE INFO

Article history:
Received 3 May 2016
Received in revised form 31 July 2016
Accepted 8 August 2016
Available online 20 August 2016

Keywords:
Sodium-ion micro-batteries
$Na_{2/3}Ni_{1/4}Mn_{3/4}O_2$
cycling performance
rate capability

ABSTRACT

Different thickness of $Na_{2/3}Ni_{1/4}Mn_{3/4}O_2$ thin films were deposited on stainless steel substrates by pulsed laser deposition technique. X-ray diffraction and field-emission scanning electron microscope results reveal that the thin film with highly preferred c-axis orientation is composed of homogeneous nano-sized grains. The charge/discharge tests indicate that the 0.55 μm thick film demonstrates a high initial discharge capacity of 175.3 $mAhg^{-1}$ and a retention of 91% after 30 cycles at a current density of 13 mAg^{-1}. Furthermore, as the current density increases from 13 to 130 mAg^{-1}, about 89% of its initial discharge capacity can be maintained, exhibiting excellent rate capability. These superior electrochemical properties would promote $Na_{2/3}Ni_{1/4}Mn_{3/4}O_2$ thin film to be a promising cathode material for sodium-ion micro-batteries.

© 2016 Elsevier Ltd. All rights reserved.

1. Introduction

Thin film-based micro-batteries have been preferred as smaller electronic power sources due to their potential applications for complementary metal oxide semiconductor (CMOS) memory chips, smart cards, remote sensors, microelectromechanical systems (MEMS), implantable medical devices [1–4]. Numerous types of thin film electrodes with high energy density and electrochemical stability have been investigated for lithium-ion batteries (LIBs) [5–8]. However, the scarcity and uneven distribution of lithium result in the pursuit of alternative energy-storage materials [9,10]. Sodium-ion batteries (SIBs) hold much promise, owing to many advantages of sodium such as high abundance, wide distribution and suitable redox potential (only about 0.3 V above that of lithium) [11–15]. As a consequence, it is necessary and desirable to produce suitable thin film electrodes for sodium-ion micro-batteries.

Nowadays, a great variety of electrode materials have been researched for rechargeable SIBs. Among them, layered sodium transition metal oxides (Na_xMO_2, $0 \leq x \leq 1$, M = Mn [16], Ni [17], Fe [18], Co [19], V [20], etc. or their combinations [21–23]) are intensely studied as potential cathode materials. In particular, the Mn-based materials $Na_xM_yMn_{1-y}O_2$, which can provide large-sized tunnels for sodium ions (de-)intercalation, have shown outstanding properties. Bruce's group synthesized P2-$Na_{0.67}MnO_2$ by slow-cooled rout, which exhibited a capacity of 175 $mAhg^{-1}$ with good capacity retention. Then they also reduced the phase transitions by substituting Mn^{3+} ions with Mg^{2+} ions, and a content of 5% was sufficient to improve the cycling stability without affecting the capacity [24]. Lee et al. found that the diffusivity of Na-ions in the P2 structure was higher than that in the corresponding O3 structured Li compounds, which confirmed the superiority of P2-$Na_{2/3}Ni_{1/3}Mn_{2/3}O_2$ [25]. Recently, Zhao et al. showed that Ti substituted P2-$Na_{2/3}Ni_{1/4}Mn_{3/4}O_2$ (Ti = 0.20) could deliver a reversible capacity of 140 $mAhg^{-1}$ with the capacity retention over 92% after 25 cycles, even cycled at high upper cut-off voltage of 4.5 V [26].

Nevertheless, to date, very little work has been reported on the electrochemical behavior of Na_xMO_2 thin film despite some interesting results on powder. Compared to conventional compacted powder electrode, the thin film has close adhesion to the substrate, which could improve the electrical conductivity of active materials and drastically reduce charge transfer barrier. Besides, the thin film electrode is more appropriate for insight into the intrinsic properties of materials since it is free of additives and binders, which is an ideal system to measure the chemical diffusion coefficient for the fundamental studies [29].

* Corresponding author. Tel.: +86 27 87543080.
E-mail addresses: yxx201730@126.com (Y. Wang), gyang@mail.hust.edu.cn (G. Yang).

http://dx.doi.org/10.1016/j.electacta.2016.08.029
0013-4686/© 2016 Elsevier Ltd. All rights reserved.

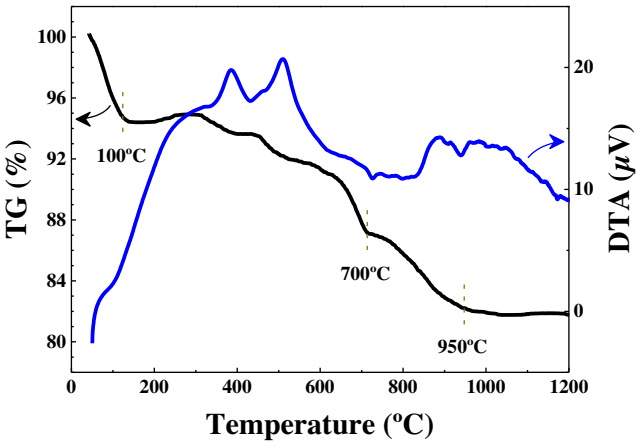

Fig. 1. TG/DTA curves of the as-prepared mixtures.

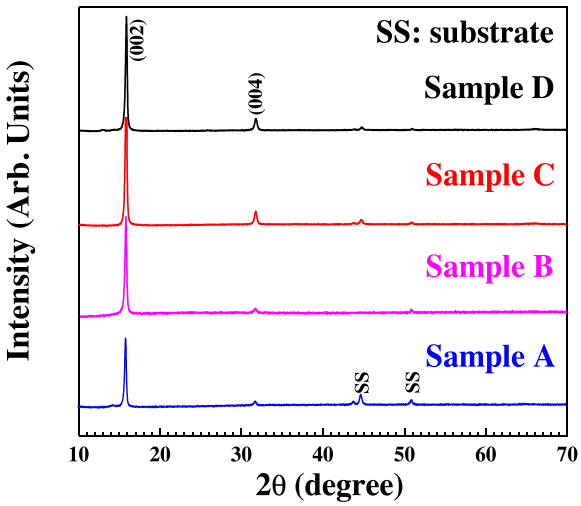

Fig. 2. XRD patterns of NNMO thin films.

In this work, in order to explore the electrochemical properties of $Na_{2/3}Ni_{1/4}Mn_{3/4}O_2$ thin films, we fabricated the samples on stainless steel substrates by pulsed laser deposition (PLD). In a variety of film-growth methods, PLD shows many advantages, for example, high texture, good crystallinity, easy to control thickness and uniformity, and direct stoichiometry transfer from the target to the film [30–32]. Electrochemical tests indicate that the 0.55 μm thick film behaves high capacity, excellent cycling performance and rate capability.

2. Experimental

The target for laser sputtering was prepared by the conventional solid state reaction method. NaOH (99.99%), MnO_2 (99.9%) and NiO (99.9%) were mixed using ball mill. These mixtures were calcined firstly at 750 °C for 24 h, then at 1000 °C for 12 h in air. A 248 nm laser beam, provided by the KrF excimer pulsed laser, was focused onto the surface of the target. The laser energy intensity and repetition frequency were 2 J/cm^2 and 10 Hz, respectively. Different thickness of $Na_{2/3}Ni_{1/4}Mn_{3/4}O_2$ (NNMO) thin films were deposited on stainless steel (SS) and SiO_2/Si (SOS) substrates at 750 °C in an oxygen partial pressure of 65 Pa for 30 min (Sample A), 60 min (Sample B), 120 min (Sample C) and 240 min (Sample D), respectively, followed by in-situ annealing for 60 min. Afterwards, all the samples were stored under an inert atmosphere.

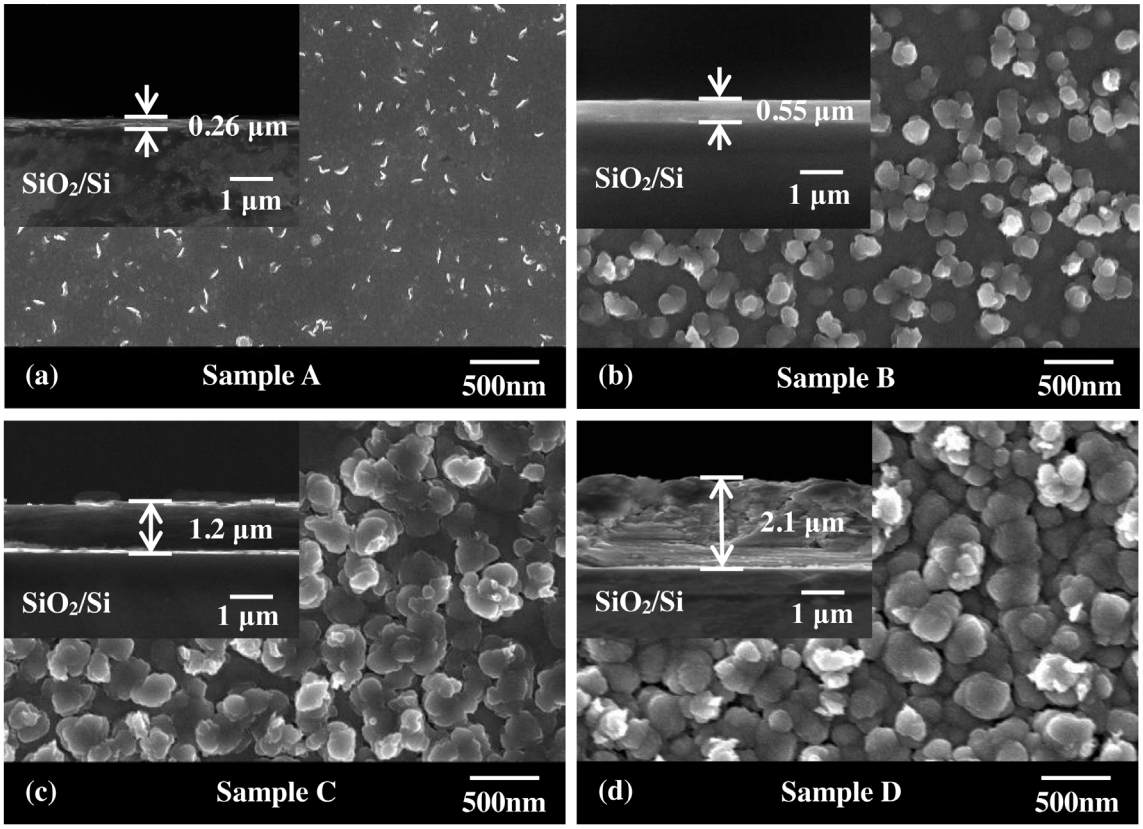

Fig. 3. FSEM images of the NNMO films on SS substrates, and (inset) cross-sectional views of the NNMO films on SiO_2/Si substrates.

Before the sintering, thermogravimetric-differential thermal (TG-DTA) data of the mixtures were obtained on a Diamond TG/DTA (PerkinElmer Instruments, Shanghai, China) at a heating rate of 20 °C/min from room temperature to 1200 °C under air atmosphere. The crystalline structure of NNMO films were characterized by X-ray diffraction (XRD, X'Pert PRO, PANalytical B.V.) with Cu Kα radiation (λ = 1.5406 Å). The XRD patterns were collected in a range of 2θ values from 10° to 70° at a scanning rate of 10° min^{-1} and a step size of 0.02°. The surface morphologies of NNMO films were studied by field-emission scanning electron microscope (FSEM, Sirion 200, FEI). The compositions of NNMO film was determined by Inductively Coupled Plasma Optical Emission Spectrometry (ICP-OES, Optima 4300DV, Perkin Elmer). All the thin films were weighted by precision electronic balance (AL104, METTLER TOLEDO, weight precision ±0.01 mg).

For the electrochemical measurements, the 2032 type coin cells were constructed by using the NNMO thin film as a working electrode, one Na disk as a counter electrode, glass fiber membrane (GF/D, Whatman) as the separator, and 1 M $NaClO_4$ in a mixture of ethylene carbonate (EC) and propylene carbonate (PC) (2:1 by volume) as the electrolyte. The Na disks were made by rolling sodium chunks into thin sheets, which were then cut into circulated plates. And, the cells were assembled in an argon-filled glove box. Galvanostatic charge/discharge measurements were performed on a Neware BTS-5V1mA battery tester (Shenzhen Neware Electronic Co. Ltd., China) at various current densities between the voltage windows of 1.5–4.3 V at room temperature.

3. Results and discussion

TG/DTA was performed on the as-prepared mixtures (NaOH, MnO_2 and NiO) to investigate the reasonable temperature for the sintering process. As shown in Fig. 1, the first weight loss before 100 °C may be due to the evaporation of water and dehydration reaction; the second weight loss between 100 and 700 °C is attributed to the primary reaction of these mixed oxide materials; the third weight loss between 700 and 950 °C is the further combustion of these compounds residues and the possible phase transformation from O-type to P-type. Above 950 °C, the mass loss is not obvious, indicating that the compounds have been completely decomposed. Based on these results, the temperature of 750 and 1000 °C are chosen for the stepwise calcination of target.

The XRD patterns of NNMO thin films with different deposition time are depicted in Fig. 2. It is clearly observed that there are only two peaks (002) and (004) in all the samples except for peaks from the SS substrate, suggesting highly preferred c-axis orientation. Also, the major diffraction peaks are well consistent with JCPDS No 54-0894, indexed to the hexagonal layered structure (P2-type) with space group P63/mmc. The film with preferred orientation, corresponding to the high symmetry of P2 structure, maybe estimate the sodium ion transfer active surface area accessible and allow sodium ions to be easier for transfer into/from electrolyte [33]. As the deposition time increases, the intensity of peaks due to (00l) becomes stronger. In addition, the atomic compositions of $Na_{2/3}Ni_{1/4}Mn_{3/4}O_2$ thin film has been verified via ICP-OES which reveals a Na: Ni: Mn ratio of 0.56: 0.26: 0.73. These metal values are close to the target.

Fig. 3 presents the FSEM images of the surface morphology and particle size of the NNMO films on SS substrates and cross-sectional views on SOS substrates. From the cross-sectional views (see the inset of Fig. 3a–d), the average thickness of Sample A, B, C and D is estimated to be about 0.26 μm, 0.55 μm, 1.2 μm and 2.1 μm, respectively. The surface of NNMO in Fig. 3 is relatively uniform with only several raised particles on it. It is obvious that the Sample A is composed of small grains with an average grain size of about 20–50 nm. As the thickness increases, the close-packed, well-defined, fairly homogeneous and larger nano-sized grains appear. This type of morphology can decrease particle agglomeration and aid in reducing the distance for ionic migration [34].

Electrochemical studies on NNMO thin-film electrodes were evaluated in sodium half cells at room temperature. Fig. 4 displays the cycle performance at a current density of 13 mAg^{-1} in the

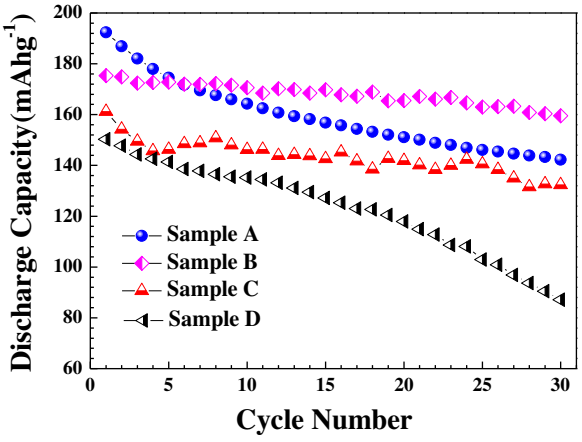

Fig. 4. Cycle performance of NNMO thin-film electrodes at a current density of 13 mAg^{-1} in the voltage range from 1.5 to 4.3 V.

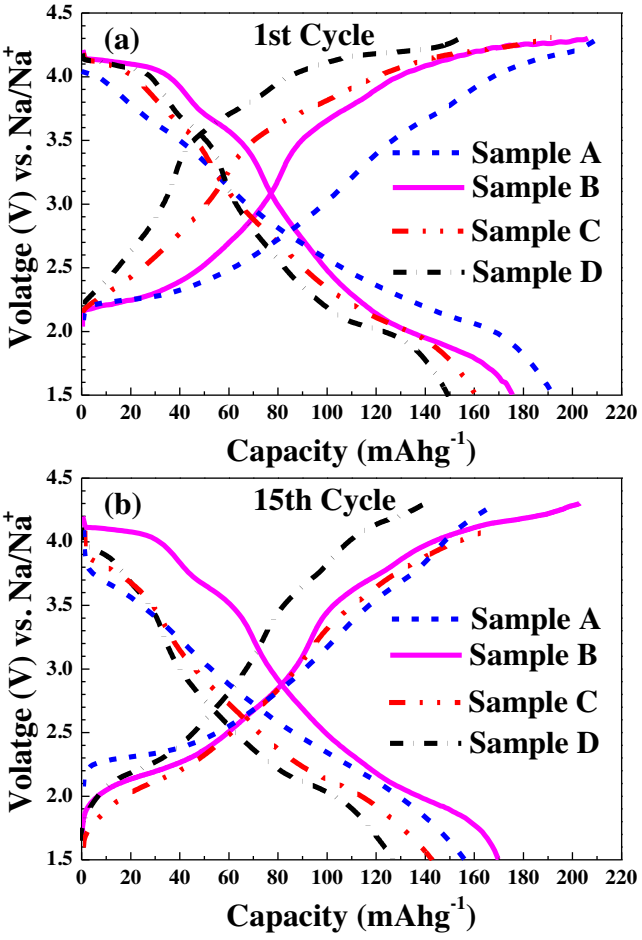

Fig. 5. Galvanostatic charge/discharge profiles at the (a) 1 st and (b) 15th cycles of NNMO thin-film electrodes.

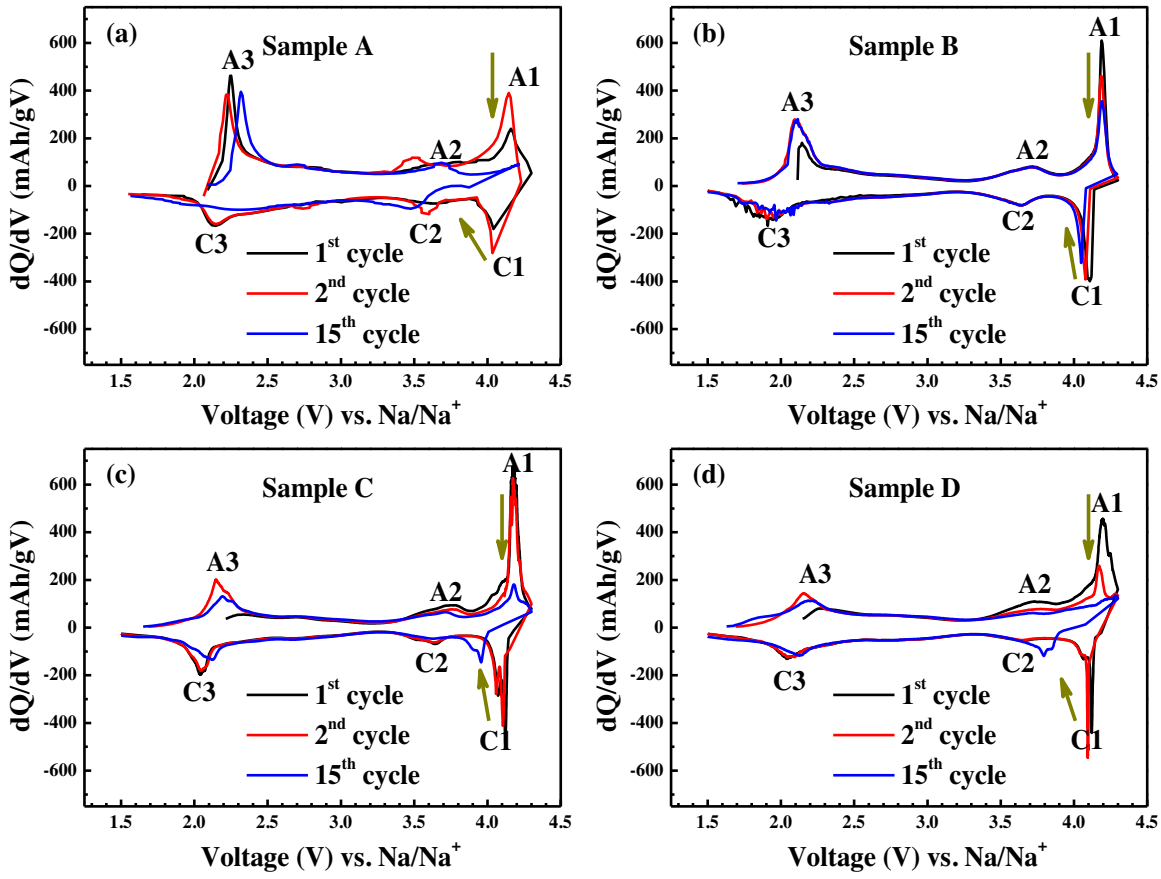

Fig. 6. The differential capacity vs. voltage curves of NNMO thin-film electrodes.

voltage range from 1.5 to 4.3 V. It is easy to see that, as the thickness increases, the discharge capacity for the first cycle is reduced obviously. At the initial cycles, the discharge capacities of Sample A, C and D show similar attenuation trend. In contrast, the Sample B holds a superior retention rate. After 30 cycles, the capacity of Sample B maintains 159.5 $mAhg^{-1}$, corresponding to 91% of its first cycle, which is higher than Sample A (142.2 $mAhg^{-1}$, 74%), C (132.3 $mAhg^{-1}$, 82%) and D (87.1 $mAhg^{-1}$, 60%). For the thinner thickness, the smaller particle size, which greatly shortens diffusion pathways for both electrons and sodium-ions, may contribute to the high initial intercalated-Na capacity and excellent cycling stability. However, if the thickness is too thin (like Sample A), the large specific surface causes more irreversible capacities to form the solid electrolyte interface film, which leads to the rapid decrease of the discharge capacity. Among them, Sample B (0.55 μm) exhibits the best cycling performance with an initial capacity of 175.3 $mAhg^{-1}$.

Fig. 5 shows the galvanostatic charge/discharge profiles for the 1st and 15th cycles. All samples show similar slopes as well as other features. Three major discharge plateaus at around 2.0, 3.5 and 4.0 V are visible at the 1st cycle in Fig. 5 (a). Obviously, the profiles of Sample B exhibit wider and higher voltage plateaus than those of others, indicating the existence of more reaction sites and smaller cell polarization. In analogy to $Na_{2/3}[Ni_{1/3}Mn_{2/3}]O_2$ [27,28], slightly decreasing the Ni content in $Na_{2/3}[Ni_{1/4}Mn_{3/4}]O_2$ would be compensated by the oxidation of Mn^{3+}, which might lead to the disappearance of 3.0 V plateau and increase participation of the Mn^{3+}/Mn^{4+} couple [26]. Furthermore, as shown in Fig. 5(b), the discharge capacities of Sample A, C and D at the 15th cycle decrease rapidly and the voltage profiles change from multi-step shape to sloping type. Nonetheless, the retained discharge capacity of Sample B can reach 97%, and no significant changes of the charge/discharge profiles are observed.

Moreover, the differential capacity vs. voltage curves in Fig. 6 clearly present the locations of the voltage plateaus. There are three pairs of well-separated peaks for all samples at the 1st cycle. The corresponding anodic and cathodic peaks are marked as A1-C1, A2-C2 and A3-C3. And, the Sample B has slightly higher central positions located at 4.19/4.13, 3.72/3.65, and 2.14/1.98 V (anodic/cathodic vs. Na/Na^+), respectively. These match well with the results in Fig. 5. In 2010, Lu et al. reported the in-situ XRD

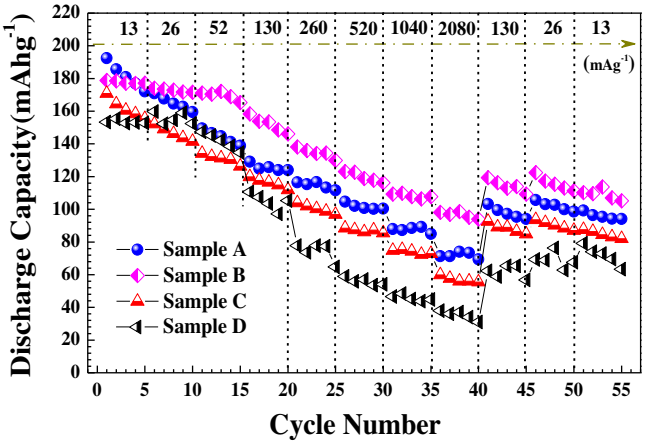

Fig. 7. Rate capability of NNMO thin-film electrodes in the voltage range from 1.5 to 4.3 V.

Table 1
Discharge capacities of NNMO thin-film electrodes.

Sample	Discharge capacities ($mAhg^{-1}$) at different discharge current densities								
	$13mAg^{-1}$ (start)	$26mAg^{-1}$	$52mAg^{-1}$	$130mAg^{-1}$	$260mAg^{-1}$	$520mAg^{-1}$	$1040mAg^{-1}$	$2080mAg^{-1}$	$13mAg^{-1}$ (end)
A	192.4	170.9	149.5	129.1	116.5	104.6	100.5	84.9	99.3
B	178.8	174.0	171.0	158.4	138.1	123.0	109.2	98.0	110.2
C	170.9	152.2	134.1	133.7	103.9	88.5	74.8	59.8	87.6
D	153.4	159.7	147.4	110.6	77.8	64.7	46.6	38.0	79.1

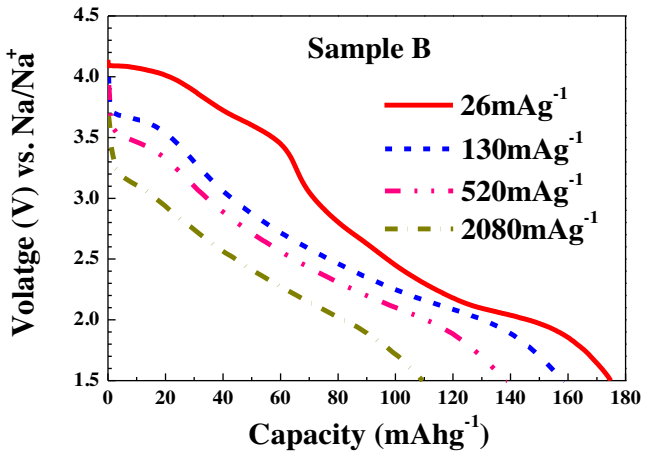

Fig. 8. Discharge curves of Sample B at different current densities.

measurement of $Na_x[Ni_{1/3}Mn_{2/3}]O_2$ during the initial charge process and revealed that this material remained in the P2 structure below 3.8 V. Also, when the electrode crossed the long plateau at 4.2 V, a new phase (O2-type structure, corresponding to $[Ni_{1/3}Mn_{2/3}]O_2$) would appear, then the P2-type fully turned to O2-type when charged to 4.4 V. Besides, the crystal structure of P2-type was gradually recovered during the sodium intercalation process [35]. It follows that the A2-C2 and A3-C3 below 3.8 V are separately associated with the redox reaction of the Ni^{2+}/Ni^{4+} and Mn^{3+}/Mn^{4+} couples, due to single-phase intercalation. And, the A1-C1 at higher potential is accompanied by structural transitions (P2-type ↔ O2-type), thus a two-phase coexistence state occurs between 4.1 and 4.3 V. Upon consecutive cycling, the C1 peak changes greatly. For Sample A, C and D in Fig. 6(a, c and d), the C1 peak at the 15th cycle shifts to lower voltage and becomes broaden until it disappears. However, for Sample B in Fig. 6(b), the intensity and location of this peak show tinier variation, suggesting the better structure stability and cycling reversibility. From dQ/dV analysis it is clear the influence of film thickness on the voltage-capacity profiles of NNMO thin-film electrodes.

For further investigation, the rate capability of NNMO thin-film electrodes were tested between 1.5 and 4.3 V at a constant charge current density of 13 mAg^{-1}, as shown in Fig. 7. In addition, Table 1 specifically lists the discharge capacities at different discharge current densities. As the current density increases to 52 mAg^{-1}, the discharge capacities of Sample A, C and D decrease quickly, while, the Sample B can keep much higher capacity of 171.0 $mAhg^{-1}$. With further increasing current density, the discharge capacity of Sample B exhibits the slowest attenuation rate, revealing the rapid transmittability of sodium ions in this film with suitable thickness and particle size. After the high rate measurement, the current density was gradually reduced back to 13 mAg^{-1}, the Sample B delivers a discharge capacity of 110.2 $mAhg^{-1}$, corresponding to 62% of its initial discharge capacity.

The corresponding voltage-capacity profiles of Sample B at different discharge current densities are displayed in Fig. 8. With increasing the current density, it exhibits these phenomena: capacity fading, lower cell voltages and no clear plateaus observed. These may be due to the increasing cell polarization and formation of an unstable stable solid electrolyte interface, which arise from the Na^+ diffusion process in the cathodes at higher current densities. Even so, it is notable that the Sample B behaves slow descent rates, indicating the good interface stability for reasonable nanoscaled thin-film sodium-ion electrodes.

4. Conclusions

Different thickness of $Na_{2/3}Ni_{1/4}Mn_{3/4}O_2$ thin films with highly preferred orientation, nano-sized grains and good crystallization were successfully deposited on SS substrates by PLD technique. The 0.55 μm thick film exhibits a higher initial discharge capacity of 175.3 $mAhg^{-1}$ and a retention of 91% after 30 cycles at a current density of 13 mAg^{-1}. Furthermore, they maintain a discharge capacity of 158.4 $mAhg^{-1}$ at a higher current density of 130 mAg^{-1}, and 110.2 $mAhg^{-1}$ can be recovered after the high current densities. We believe that the further optimization of the sodium ion diffusion channel and structure stability would drive $Na_{2/3}Ni_{1/4}Mn_{3/4}O_2$ thin film to be a suitable and efficient cathode material for sodium-ion micro-batteries.

Acknowledgments

The authors acknowledge the Analytical and Testing Center in Huazhong University of Science and Technology for TG/DTA, XRD, and FSEM measurements. The finance support from the National Natural Science Foundation of China (11374114, 10974062) is also acknowledged.

References

[1] C. Julien, A. Gorenstein, Materials Design and Optimization for Thin-Film Microbatteries, Ionics 1 (1995) 193.
[2] T. Jimbo, P. Kim, K. Suu, Production Technology for Thin-film Lithium Secondary Battery, Energy Procedia 14 (2012) 1574.
[3] W. Xiong, Q. Xia, H. Xia, Three-dimensional self-supported metal oxides as cathodes for microbatteries, Functional Materials Letters 7 (2014) 1430003.
[4] B.L. Ellis, P. Knauth, T. Djenizian, Three-Dimensional Self-Supported Metal Oxides for Advanced Energy Storage, Advanced Materials 26 (2014) 3368.
[5] X. Liu, H. Xu, Y. Huang, X. Hu, Direct planting of ultrafine $MoO_{2+\delta}$ nanoparticles in carbon nanofibers by electrospinning: self-supported mats as binder-free and long-life anodes for lithium-ion batteries, Physical Chemistry Chemical Physics 18 (2016) 19832.
[6] B.J. Neudecker, R.A. Zuhr, J.B. Bates, Lithium silicon tin oxynitride (Li_ySiTON): high-performance anode in thin-film lithium-ion batteries for microelectronics, Journal of Power Sources 81–82 (1999) 27.
[7] N.A. Kyerematen, Self-Organised TiO_2 Nanotubes for 2D or 3D Li-Ion Microbatteries, ChemElectroChem 1 (2014) 1442.
[8] B.J. Cabana, L. Monconduit, D. Larcher, M.R. Palacín, Beyond Intercalation-Based Li-Ion Batteries: The State of the Art and Challenges of Electrode Materials Reacting Through Conversion Reactions, Advanced Materials 22 (2010) E170.
[9] J.-M. Tarascon, M. Armand, Issues and challenges facing rechargeable lithium batteries, Nature 414 (2001) 359.
[10] J.B. Goodenough, Y. Kim, Challenges for Rechargeable Li Batteries, Chemistry of Materials 22 (2009) 587.

[11] S.P. Ong, V.L. Chevrier, G. Hautier, A. Jain, C. Moore, S. Kim, X. Ma, G. Ceder, Voltage, stability and diffusion barrier differences between sodium-ion and lithium-ion intercalation materials, Energy & Environmental Science 4 (2011) 3680.
[12] V. Palomares, P. Serras, I. Villaluenga, K.B. Hueso, J. Carretero-González, T. Rojo, Na-ion batteries, recent advances and present challenges to become low cost energy storage systems, Energy & Environmental Science 5 (2012) 5884.
[13] B.L. Ellis, L.F. Nazar, Sodium and sodium-ion energy storage batteries, Current Opinion in Solid State and Materials Science 16 (2012) 168.
[14] M.D. Slater, D. Kim, E. Lee, C.S. Johnson, Sodium-Ion Batteries, Advanced Functional Materials 23 (2013) 947.
[15] H. Pan, Y.-S. Hu, L. Chen, Room-temperature stationary sodium-ion batteries for large-scale electric energy storage, Energy & Environmental Science 6 (2013) 2338.
[16] A. Caballero, L. Hernán, J. Morales, L. Sánchez, J. Santos Peña, M.A.G. Aranda, Synthesis and characterization of high-temperature hexagonal P2-$Na_{0.6}MnO_2$ and its electrochemical behaviour as cathode in sodium cells, Journal of Materials Chemistry 12 (2002) 1142.
[17] K. Park, B.-C. Yu, J.B. Goodenough, Electrochemical and Chemical Properties of Na_2NiO_2 as a Cathode Additive for a Rechargeable Sodium Battery, Chemistry of Materials 27 (2015) 6682.
[18] J. Zhao, L. Zhao, N. Dimov, S. Okada, T. Nishida, Electrochemical and Thermal Properties of α-$NaFeO_2$ Cathode for Na-Ion Batteries, Journal of The Electrochemical Society 160 (2013) A3077.
[19] R. Berthelot, D. Carlier, C. Delmas, Electrochemical investigation of the P2-Na_xCoO_2 phase diagram, Nature Materials 10 (2011) 74.
[20] M. Guignard, C. Didier, J. Darriet, P. Bordet, E. Elkaïm, C. Delmas, P2-Na_xVO_2 system as electrodes for batteries and electron-correlated materials, Nature Materials 12 (2013) 74.
[21] N. Yabuuchi, M. Kajiyama, J. Iwatat, H. Nishikawa, S. Hitomi, R. Okuyama, R. Usui, Y. Yamada, S. Komaba, P2-type $Na_x[Fe_{1/2}Mn_{1/2}]O_2$ made from earth-abundant elements for rechargeable Na batteries, Nature Materials 11 (2012) 512.
[22] X. Xu, S. Ji, R. Gao, J. Liu, Facile synthesis of P2-type $Na_{0.4}Mn_{0.54}Co_{0.46}O_2$ as a high capacity cathode material for sodium-ion batteries, RSC Advances 5 (2015) 51454.
[23] E. Talaie, V. Duffort, H.L. Smith, B. Fultz, L.F. Nazar, Structure of the high voltage phase of layered P2-$Na_{2/3-z}[Mn_{1/2}Fe_{1/2}]O_2$ and the positive effect of Ni substitution on its stability, Energy & Environmental Science 8 (2015) 2512.
[24] J. Billaud, G. Singh, A.R. Armstrong, E. Gonzalo, V. Roddatis, M. Armand, T. Rojo, P.G. Bruce, $Na_{0.67}Mn_{1-x}Mg_xO_2$ ($0 \leq x \leq 0.2$): a high capacity cathode for sodium-ion batteries, Energy & Environmental Science 7 (2014) 1387.
[25] D.H. Lee, J. Xu, Y.S. Meng, An advanced cathode for Na-ion batteries with high rate and excellent structural stability, Physical Chemistry Chemical Physics 15 (2013) 3304.
[26] W. Zhao, A. Tanaka, K. Momosaki, S. Yamamoto, F. Zhang, Q. Guo, H. Noguchi, Enhanced electrochemical performance of Ti substituted P2-$Na_{2/3}Ni_{1/4}Mn_{3/4}O_2$ cathode material for sodium ion batteries, Electrochimica Acta 170 (2015) 171.
[27] H. Wang, B. Yang, X.-Z. Liao, J. Xu, D. Yang, Y.-S. He, Z.-F. Ma, Electrochemical properties of P2-$Na_{2/3}[Ni_{1/3}Mn_{2/3}]O_2$ cathode material for sodium ion batteries when cycled in different voltage ranges, Electrochimica Acta 113 (2013) 200.
[28] Y. Wen, B. Wang, G. Zeng, K. Nogita, D. Ye, L. Wang, Electrochemical and Structural Study of Layered P2-Type $Na_{2/3}Ni_{1/3}Mn_{2/3}O_2$ as Cathode Material for Sodium-Ion Battery, Chemistry-An Asian Journal 10 (2015) 661.
[29] T. Shibata, Y. Fukuzumi, W. Kobayashi, Y. Moritomo, Fast discharge process of layered cobalt oxides due to high Na^+ diffusion, Scientific reports 5 (2015) 9006.
[30] Y. Wang, G. Yang, Z. Yang, L. Zhang, M. Fu, H. Long, Z. Li, Y. Huang, P. Lu, High power and capacity of $LiNi_{0.5}Mn_{1.5}O_4$ thin films cathodes prepared by pulsed laser deposition, Electrochimica Acta 102 (2013) 416.
[31] Y. Wang, Q. Peng, G. Yang, Z. Yang, L. Zhang, H. Long, Y. Huang, P. Lu, High-stability 5 V spinel $LiNi_{0.5}Mn_{1.5}O_4$ sputtered thin film electrodes by modifying with aluminium oxide, Electrochimica Acta 136 (2014) 450.
[32] T. Shibata, W. Kobayashi, Y. Moritomo, Intrinsic rapid Na^+ intercalation observed in Na_xCoO_2 thin film, AIP Advances 3 (2013) 032104.
[33] S. Takeuchi, H. Tan, K.K. Bharathi, G.R. Stafford, J. Shin, S. Yasui, I. Takeuchi, L.A. Bendersky, Epitaxial $LiCoO_2$ Films as a Model System for Fundamental Electrochemical Studies of Positive Electrodes, ACS Applied Materials & Interfaces 7 (2015) 7901.
[34] K. Kaliyappan, J. Liu, A. Lushington, R. Li, X. Sun, Highly Stable $Na_{2/3}(Mn_{0.54}Ni_{0.13}Co_{0.13})O_2$ Cathode Modified by Atomic Layer Deposition for Sodium-Ion Batteries, ChemSusChem 8 (2015) 2537.
[35] Z. Lu, J.R. Dahn, In Situ X-Ray Diffraction Study of P2-$Na_{2/3}[Ni_{1/3}Mn_{2/3}]O_2$, Journal of The Electrochemical Society 148 (2001) A1225.